

Article

Theoretical and Experimental Study of LiBH₄-LiCl Solid Solution

Olena Zavorotynska ^{1,*}, Marta Corno ¹, Eugenio Pinatel ¹, Line H. Rude ², Piero Ugliengo ¹,
Torben R. Jensen ² and Marcello Baricco ¹

¹ Dipartimento di Chimica and NIS, Università degli Studi di Torino, via Giuria 7/9, Torino 10125, Italy; E-Mails: marta.corno@unito.it (M.C.); eugenio.pinel@unito.it (E.P.); piero.ugliengo@unito.it (P.U.); marcello.baricco@unito.it (M.B.)

² Center for Materials Crystallography (CMC), Interdisciplinary Nanoscience Center (iNANO) and Department of Chemistry, Aarhus University, Langelandsgade 140, DK-8000 Århus C, Denmark; E-Mails: line@inano.au.dk (L.H.R.); trj@chem.au.dk (T.R.J.)

* Author to whom correspondence should be addressed; E-Mail: olena.zavorotynska@unito.it; Tel.: +39-011-670-7840; Fax: +39-011-236-4596.

Received: 16 February 2012; in revised form: 7 March 2012 / Accepted: 13 March 2012 /

Published: 21 March 2012

Abstract: Anion substitution is at present one of the pathways to destabilize metal borohydrides for solid state hydrogen storage. In this work, a solid solution of LiBH₄ and LiCl is studied by density functional theory (DFT) calculations, thermodynamic modeling, X-ray diffraction, and infrared spectroscopy. It is shown that Cl substitution has minor effects on thermodynamic stability of either the orthorhombic or the hexagonal phase of LiBH₄. The transformation into the orthorhombic phase in LiBH₄ shortly after annealing with LiCl is for the first time followed by infrared measurements. Our findings are in a good agreement with an experimental study of the LiBH₄-LiCl solid solution structure and dynamics. This demonstrates the validity of the adopted combined theoretical (DFT calculations) and experimental (vibrational spectroscopy) approach, to investigate the solid solution formation of complex hydrides.

Keywords: lithium borohydride; anion substitution; CRYSTAL code; infrared spectroscopy; CALPHAD

1. Introduction

Mixtures of metal borohydrides with halides have recently evoked careful attention as candidates for hydrogen storage materials [1–7] and novel solid-state lithium electrolytes [8–11]. Whereas the improvement in the hydrogen absorption and release kinetics and thermodynamics of these materials is still under investigation, their recently-discovered high ionic conductivity opens new horizons for applications. Metal borohydride mixtures with halides are proved to form solid solutions [7,10–13]. Anion substitution changes the site symmetry of the BH_4^- ions, which is immediately reflected in the vibrational spectra. For example, in the $\text{LiBH}_4\text{-LiI}$ and $\text{LiBH}_4\text{-LiBr}$ solid solutions [14,15], Br^- and I^- stabilize the high temperature hexagonal phase of LiBH_4 at room temperature. The phase transformation from *o*- to *h*- LiBH_4 caused by anion exchange is shown to modify substantially the profile of the BH_4^- infrared vibrations.

Periodic *ab initio* CRYSTAL code [16] has already been successfully applied in a number of studies dealing with the computational prediction of solid solution formation, both for simple and complex hydrides [2,17]. The starting structures are taken from the experimental data collected in the Inorganic Crystal Structure Database [18] and are fully optimized to get the minimum energy geometry. Accurate calculations of the vibrational frequencies on the optimized system geometry allowed us to simulate infrared/Raman spectra and to draw a punctual comparison with the experimental measurements [19]. The comparison can be very useful in assigning complex spectral patterns of novel compounds and also in stating whether the solid solution has formed or not. Moreover, by computing vibrations and applying the equations of statistical mechanics, thermodynamic properties can be evaluated, such as solid solution formation enthalpy, entropy, free energy and heat capacity at the desired temperatures. In particular, in the case of lithium borohydride, some of us have performed DFT calculations on the orthorhombic phase, mixed with LiBF_4 [2]. In that case, the major issue has regarded the calculation of a large number of possible configurations, because fluorine is substituting hydrogen atom(s) inside the borohydride tetrahedral units. Conversely, in the case of other halide ions, such as Cl^- , the entire BH_4^- group is substituted because of the correspondent ionic radii ($r = 1.81 \text{ \AA}$ for Cl^- and 2.05 \AA for BH_4^- [12,20]).

In this work, we present the study on the $\text{LiBH}_4\text{-LiCl}$ system, utilizing attenuated total reflection infrared spectroscopy (IR-ATR), powder X-ray diffraction (PXRD), DFT calculations with CRYSTAL code and thermodynamic modeling.

2. Results and Discussion

2.1. Optimized Structures of *o*- $\text{LiBH}_4\text{-Cl}$ and *h*- $\text{LiBH}_4\text{-Cl}$ Solid Solutions

Pure orthorhombic (*o*- LiBH_4 , *Pnma* space group) and hexagonal (*h*- LiBH_4 , *P6₃mc* space group) structures of LiBH_4 were optimized at the DFT-Perdew-Burke-Ernzerhof (DFT-PBE) level of theory, starting from the experimental coordinates [21]. The optimized unit cell structures are shown in Figure 1, whereas the most important structural parameters are summarized in Table 1 in comparison with experimental data.

Figure 1. Optimized crystal structures of pure and Cl-substituted unit cells of orthorhombic and hexagonal LiBH_4 . Positions of H1, H2, and H3 are shown for the $x = 0$.

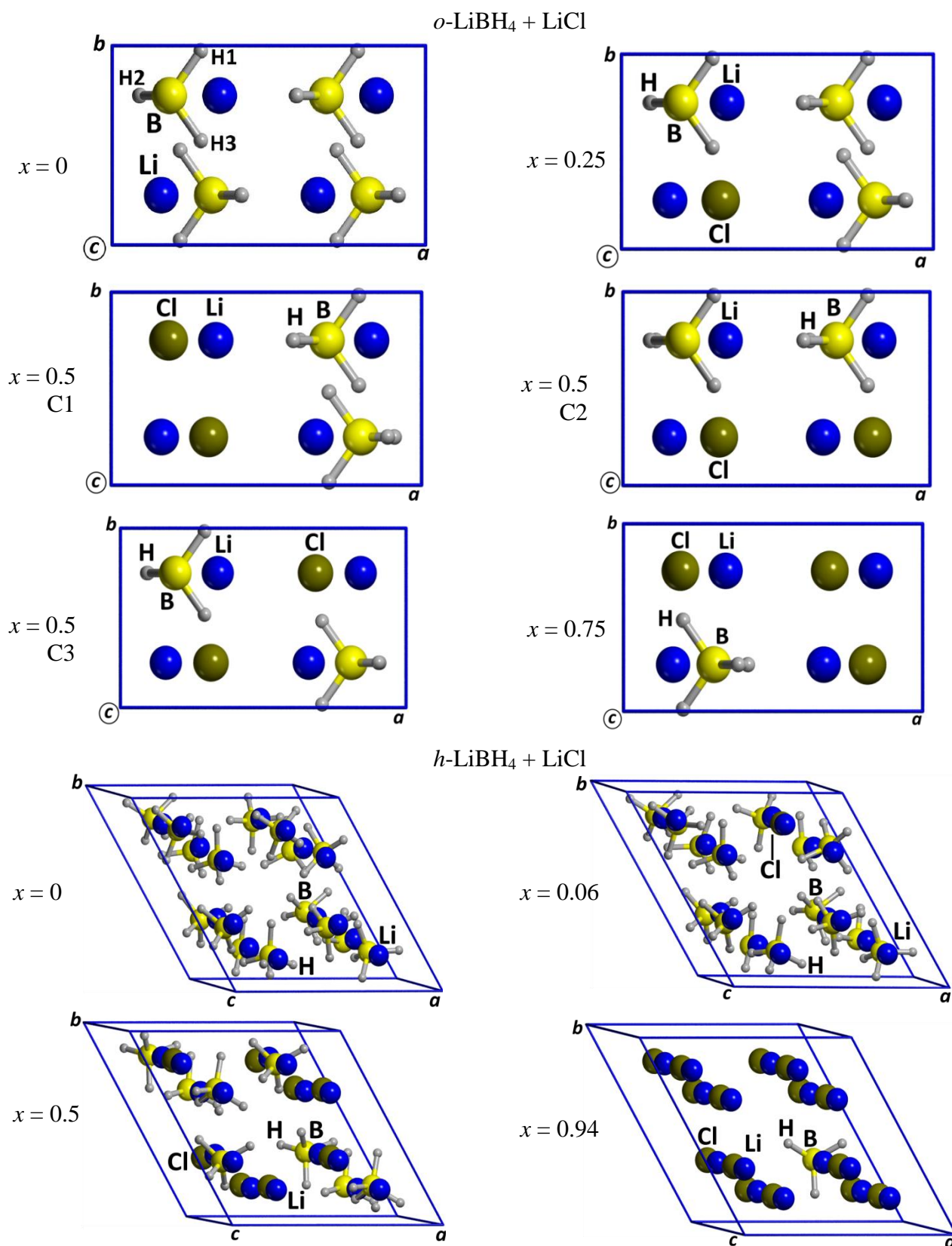


Table 1. Lattice parameters and most relevant bond lengths for optimized DFT models of pure and Cl-substituted orthorhombic and hexagonal phases of LiBH₄, compared to the corresponding experimental values, if available. B-H distances and <B-H> average distances are expressed in Å, cell volume in Å³, the average bond angles <HBH> in degrees. Structures are displayed in Figure 1.

| <i>o</i> -LiBH ₄ <i>Pnma</i> | <i>a</i> | <i>b</i> | <i>c</i> | Volume | B-H1 | B-H2 | B-H3 | <B-H> | <HBH> |
|---------------------------------------------------------------------------------|----------|----------|----------|--------|-------|-------|-------|-------|-------|
| Exp. ^a | 7.121 | 4.406 | 6.674 | 209.4 | 1.213 | 1.224 | 1.208 | 1.215 | 109.3 |
| DFT | 7.328 | 4.379 | 6.494 | 208.4 | 1.230 | 1.233 | 1.229 | 1.231 | 109.3 |
| DFT -LiBH ₄ + LiCl | | | | | | | | | |
| <i>o</i> -Li(BH ₄) _{0.75} Cl _{0.25} | 7.255 | 4.314 | 6.472 | 202.6 | 1.232 | 1.235 | 1.228 | 1.232 | 108.8 |
| <i>o</i> -Li(BH ₄) _{0.5} Cl _{0.5} /C ₁ | 7.111 | 4.245 | 6.538 | 197.3 | 1.228 | 1.234 | 1.225 | 1.229 | 109.0 |
| <i>o</i> -Li(BH ₄) _{0.5} Cl _{0.5} /C ₂ | 7.207 | 4.250 | 6.425 | 196.8 | 1.228 | 1.235 | 1.228 | 1.230 | 109.0 |
| <i>o</i> -Li(BH ₄) _{0.5} Cl _{0.5} /C ₃ | 7.181 | 4.241 | 6.477 | 197.2 | 1.231 | 1.234 | 1.227 | 1.232 | 108.0 |
| <i>o</i> -Li(BH ₄) _{0.25} Cl _{0.75} | 7.079 | 4.161 | 6.538 | 192.7 | 1.226 | 1.234 | 1.226 | 1.232 | 108.9 |
| <i>h</i> -LiBH ₄ <i>P6₃mc</i> | | | | | | | | | |
| Exp. ^a | 4.267 | 4.267 | 6.922 | 109.1 | 0.962 | 1.024 | 1.024 | 1.003 | 108.4 |
| DFT | 4.216 | 4.216 | 6.291 | 96.8 | 1.220 | 1.223 | 1.223 | 1.222 | 109.4 |
| DFT supercell | 8.297 | 8.289 | 13.333 | 793.2 | - | - | - | 1.229 | 109.5 |
| DFT <i>h</i> -LiBH ₄ + LiCl | | | | | | | | | |
| <i>h</i> -Li(BH ₄) _{0.94} Cl _{0.06} | 8.256 | 8.274 | 13.238 | 782.8 | - | - | - | 1.229 | 109.5 |
| <i>h</i> -Li(BH ₄) _{0.5} Cl _{0.5} | 8.016 | 8.067 | 12.740 | 718.1 | - | - | - | 1.228 | 109.5 |
| <i>h</i> -Li(BH ₄) _{0.06} Cl _{0.94} | 7.886 | 7.888 | 12.493 | 672.9 | 1.220 | 1.223 | - | 1.222 | 109.5 |

^a Ref. [21].

For the orthorhombic crystal, a systematic overestimation of the B-H bond length is observed, as already pointed out in literature [2,19], which however does not significantly affect the unit cell volume.

The hexagonal phase is stable at high temperature ($T \geq 381$ K) [12]. Therefore, without inclusion of temperature effects, full geometry optimization starting from the experimental structure dramatically distorts the internal geometry and the cell volume, as reported in Table 1. Indeed, for the unit cell of *h*-LiBH₄, frequency calculation at Gamma point on the optimized structure reveals six imaginary frequencies, showing the instability of this phase when temperature is not taken into account. Maintaining the cell parameters fixed at the experimental values does not remove the structural instability, as the internal atomic displacements are still very large, as shown also by Miwa *et al.* [22], due to the dynamic disorder of BH₄⁻ units [23]. In order to overcome these difficulties and, moreover, to simulate solid solutions, a supercell approach was adopted in the case of *h*-LiBH₄, considering a larger and more representative scenario (for the original cell $Z = 2 \rightarrow 12$ atoms, while in the supercell $Z = 16 \rightarrow 96$ atoms). In this operation of doubling each cell vector, symmetry is completely lost and borohydride tetrahedra are free to rotate, so removing the phonon instability found in the single unit cell. Indeed, when computing frequency values for the hexagonal supercell, only one imaginary mode is found at -20 cm⁻¹. In the following, to avoid numerical problems due to the variable number of imaginary frequencies for the structures, we have used the whole set of frequencies by considering also the imaginary values (by using their absolute value in the statistical thermodynamic formulae) for the calculation of the zero point energy (ZPE) and enthalpy corrections, as described below.

The relative energy stabilities calculated for the two phases favor the orthorhombic structure with respect to the hexagonal, as expected, but their enthalpy difference ($^{\text{ORTHO}} - ^{\text{HEX}} \Delta H = 10 \text{ kJ}\cdot\text{mol}^{-1}$ per formula unit) overestimates experimental measurements [24,25], due to the instability of the hexagonal model.

Even if the stable LiCl polymorph at room temperature is cubic, corresponding structures were obtained for both the orthorhombic and hexagonal phases as the full substitution of BH_4^- with chlorine. The difference in enthalpy for the three phases of LiCl was calculated for the phase diagram calculation, giving $^{\text{CUBIC}} - ^{\text{ORTHO}} \Delta H = 21.8 \text{ kJ}\cdot\text{mol}^{-1}$ and $^{\text{CUBIC}} - ^{\text{HEX}} \Delta H = 15.1 \text{ kJ}\cdot\text{mol}^{-1}$.

The simulation of orthorhombic solid solution $o\text{-Li}(\text{BH}_4)_{1-x}\text{Cl}_x$, where four borohydride units are present in the $o\text{-LiBH}_4$ unary cell, was performed, considering three compositions with molar fraction of chlorine, x , equal to 0.25, 0.50 and 0.75. The corresponding unary cells are reported in Figure 1. For $x = 0.5$, three non-equivalent configurations were computed, namely C1, C2 and C3, as shown in Figure 1. Among them, C3 structure turned out to be the most stable, because of the largest Cl-Cl distance. Conversely, for the hexagonal solid solution $h\text{-Li}(\text{BH}_4)_{1-x}\text{Cl}_x$, due to the large size of the supercell, only three compositions have been considered, that are $\text{Li}(\text{BH}_4)_{0.94}\text{Cl}_{0.06}$, $\text{Li}(\text{BH}_4)_{0.5}\text{Cl}_{0.5}$, and $\text{Li}(\text{BH}_4)_{0.06}\text{Cl}_{0.94}$.

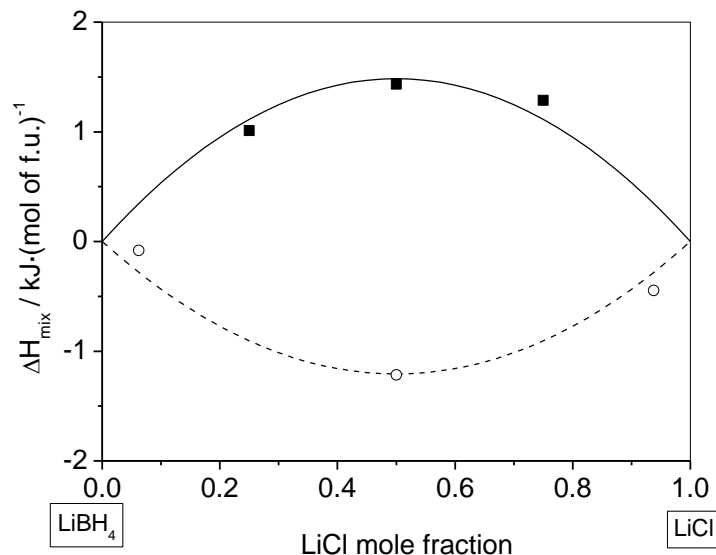
For the orthorhombic solid solutions, the unit cell volume decreases with the increase of Cl substitution, as expected, with a maximum variation of about 10% for the highest chlorine content ($x = 0.75$). For the hexagonal structures, the volume decreases as a function of Cl content, with a maximum variation of about 13% for $x = 0.94$. It can be mentioned here that the calculated cell volume reduction for the Cl-substituted $o\text{-LiBH}_4$ and $h\text{-LiBH}_4$ correlates well with the experimentally observed values [12].

Thermal entropy was calculated for each composition using classical statistical thermodynamic formulae. As it was computed using the harmonic set of frequencies, the hindered BH_4^- rotation is included, as well as the frustrated translation of the substituting Cl. It turned out that the hindered BH_4^- soft rotational motion is compensated by the frustrated translation of the substituting Cl ion, so that the thermal entropy contribution is very small, well below the contribution due to the ideal configurational entropy.

2.2. Thermodynamics of the Solid Solution Formation

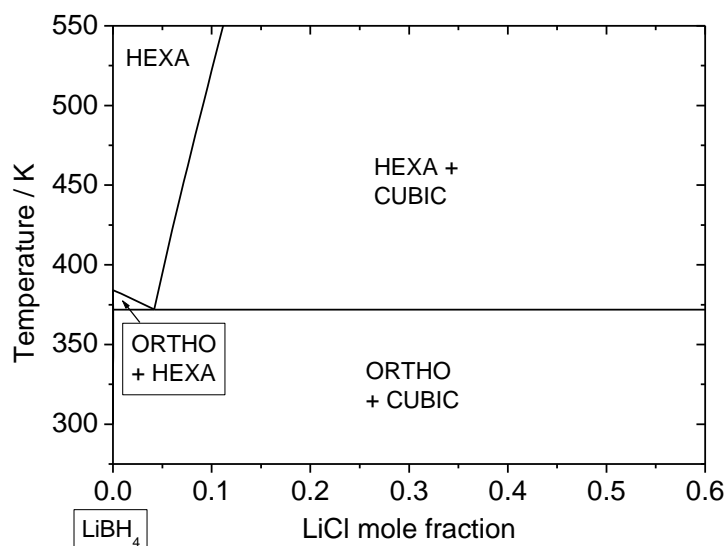
The enthalpy of mixing was computed at room temperature for the models shown in Figure 1. The obtained results are shown in Figure 2 as a function of the increasing LiCl mole fraction. According to simulations, $o\text{-LiBH}_4$ is slightly destabilized by the substitution of chloride inside the lattice, since computed enthalpy of mixing (ΔH_{mix}) values are positive and small (less than 2 kJ mol^{-1} per formula unit). On the contrary, in the hexagonal phase, the enthalpy of mixing shows slightly negative values, less than -1 kJ mol^{-1} per formula unit, so that the $h\text{-LiBH}_4$ is, to some extent, stabilized by LiCl. As stated above, the thermal entropy contribution is very small, so ideal entropy of mixing (ΔS_{mix}) has been considered for free energy calculations. When ΔH_{mix} and $-T\Delta S_{\text{mix}}$ terms are summed up at room temperature, the free energy of mixing (ΔG_{mix}) becomes close to zero for the orthorhombic phase and slightly negative for the hexagonal phase for all compositions.

Figure 2. Enthalpy of mixing for the orthorhombic and hexagonal LiBH₄-LiCl solid solutions as a function of LiCl mole fraction. *Ab initio* results are reported as squares (ortho) and circles (hexa). Results of CALPHAD modeling are represented by lines (continuous = ortho, dashed = hexa).



In order to describe thermodynamic behavior of the LiBH₄-LiCl system, the CALPHAD approach [26] was used. Due to the lack of thermodynamic data for the LiBH₄-LiCl liquid mixture, the phase diagram was evaluated, neglecting the liquid phase, and it is considered only below the melting temperature of LiBH₄. The presence of an attractive interaction in the liquid state could induce a stabilization of the liquid phase below the melting temperatures of pure components, as found experimentally by *in situ* X-ray diffraction [12].

On the basis of the evaluated thermodynamic parameters, the pseudo binary phase diagram for the LiBH₄-LiCl system has been calculated and the results shown in Figure 3. The calculated solubility of Cl into *o*-LiBH₄ is rather low and it reaches a value $x = 0.1$ at about 500 K for the *h*-LiBH₄ phase. A eutectoid phase transition is calculated at 372 K and $x = 0.04$. The phase diagram behavior is very sensitive to both lattice stabilities (*i.e.*, free energy difference between different phases of the pure components) as well as to the free energy of mixing. The very strong instability, predicted for the metastable *o*-LiCl ($^{\text{CUBIC}} - ^{\text{ORTHO}} \Delta H = 21.8 \text{ kJ}\cdot\text{mol}^{-1}$), and the calculated nearly zero ΔG_{mix} , prevent any relevant solubility of Cl inside the orthorhombic phase. The negative ΔG_{mix} for the hexagonal solid solution and a more stable *h*-LiCl, if compared to the orthorhombic one ($^{\text{HEX}} - ^{\text{ORTHO}} \Delta H = 6.7 \text{ kJ}\cdot\text{mol}^{-1}$), allow for the stabilization of the hexagonal phase with respect to the orthorhombic one when Cl is added. Of course, a lower value of $^{\text{HEX}} - ^{\text{ORTHO}} \Delta H$ and a more negative enthalpy of mixing for the hexagonal phase would promote a higher solubility of Cl in *h*-LiBH₄ phase.

Figure 3. Calculated LiBH₄-LiCl pseudo binary phase diagram.

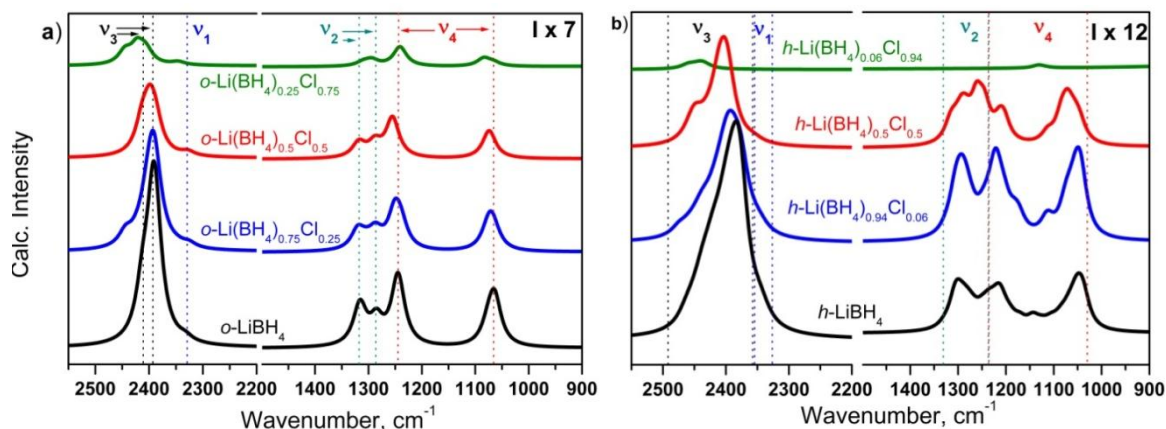
2.3. Structural Properties of *o*-Li(BH₄)_{1-x}Cl_x and *h*-Li(BH₄)_{1-y}Cl_y

2.3.1. Computational Study of the *o*-Li(BH₄)_{1-x}Cl_x and *h*-Li(BH₄)_{1-y}Cl_y Vibrational Properties

In the mid-infrared region the vibrational spectra of LiBH₄, orthorhombic and hexagonal phases exhibit stretching (ν_1 , ν_3), bending (ν_2 , ν_4) and combinational (not accounted for in the computed spectra) modes of the BH₄⁻ anions (Figure 4) [19,27–30]. The modes ν_3 and ν_4 are triply degenerate in free tetrahedral BH₄⁻ ions, and the ν_2 is doubly degenerate. Due to the different BH₄⁻ site symmetry in the *Pnma* and *P6₃mc* space groups, C_s and C_{3v} respectively, vibrational spectra of *h*-LiBH₄ are expected to be simpler, since the ν_2 mode remains degenerate and both ν_3 , ν_4 split into only two components each. The computed IR spectrum of the *h*-LiBH₄ supercell, however, is much more complex, due to the absence of any symmetry at all and 32 BH₄⁻ ions in the cell: see Figure 4b. Nevertheless, several observations can be made.

Substitution of BH₄⁻ with Cl⁻ in the unit cell of *o*-LiBH₄ does not modify significantly its IR vibrations. Stretching ν_3 and bending ν_4 modes of BH₄⁻ appear to be the most sensitive to the Cl⁻ substitution, moving to higher frequencies by $\Delta\nu = +10\dots+35$ cm⁻¹ (Figure 4a). The ν_1 and ν_2 modes are the least affected by the presence of Cl⁻, being shifted only with the highest amount of Cl⁻ in the unit cell ($x = 0.75$). These negligible modifications in the BH₄⁻ vibrational profile can be explained by the BH₄⁻ low site symmetry in pure and all the Cl-substituted unary cells of *o*-Li(BH₄)_{1-x}Cl_x, and that the substitution does not cause a significant change in the number of IR-active peaks. Since the symmetry in the supercell of the *h*-LiBH₄ and *h*-Li(BH₄)_{1-y}Cl_y is completely removed, the spectra of all compounds on the Figure 4b appear to be much more complex than are expected for the *h*-LiBH₄ unary cell. Stretching modes in the 2500–2300 cm⁻¹ region evidently shift to higher wavenumbers with increasing Cl⁻ concentration. Apparently, it is difficult to distinguish between the spectra of pure and Cl-substituted *o*-LiBH₄ or *h*-LiBH₄ when the molar concentration of Cl⁻ is small (compare black and blue curves in Figure 4).

Figure 4. Computed infrared spectra of Cl^- substitution into the LiBH_4 (a) Orthorhombic, positions of the fundamental modes in pure $o\text{-LiBH}_4$ are shown by dotted lines; (b) Hexagonal, borders of the regions of the fundamental modes in pure $h\text{-LiBH}_4$ are shown by dotted lines (for clearness, the positions, since there are too many modes). Intensity in the bending regions $1500\text{--}900\text{ cm}^{-1}$ borders of the regions are shown instead of the is expanded for clarity.



Orimo *et al.* [29] suggested a correlation between the position of the ν_1 and ν_2 modes and the stability in the Li, Na, K, Rb, Cs borohydrides: in the most stable, CsBH_4 ν_2 has the lowest energy of vibrations. In this way, the almost unaffected position of the ν_1 and ν_2 modes in the Cl-substituted LiBH_4 can be interpreted as evidence of a minor effect of the chlorine substitution on the stability of LiBH_4 .

2.3.2. Experimental Study of $\text{LiBH}_4\text{-LiCl}$ Mixture and Solid Solution

The structure and vibrations of $\text{LiBH}_4\text{-LiCl}$ mixture (1:1) were studied by powder X-ray diffraction and infrared spectroscopy. No chlorine substitution is found after hand mixing of the sample, as expected [12], (Figure 5a), whereas after annealing, a small amount of chlorine is found both in the hexagonal and orthorhombic phases of LiBH_4 (Figure 5b, Table 2).

Figure 5. Rietveld refinement profiles of (a) $\text{LiBH}_4\text{-LiCl}$ (1:1) hand-mixed mixture, measured by powder X-ray diffraction (Cu $\text{K}\alpha_1$ and $\text{K}\alpha_2$) at $T = 25\text{ }^\circ\text{C}$, top bars: LiCl , bottom bars: $o\text{-LiBH}_4$; (b) $\text{LiBH}_4\text{-LiCl}$ (1:1) hand-mixed mixture after annealing, within 30 min after the infrared measurements, top bars: LiCl , middle bars: $o\text{-Li}(\text{BH}_4)_{0.90}\text{Cl}_{0.10}$; bottom bars: $h\text{-Li}(\text{BH}_4)_{0.96}\text{Cl}_{0.04}$.

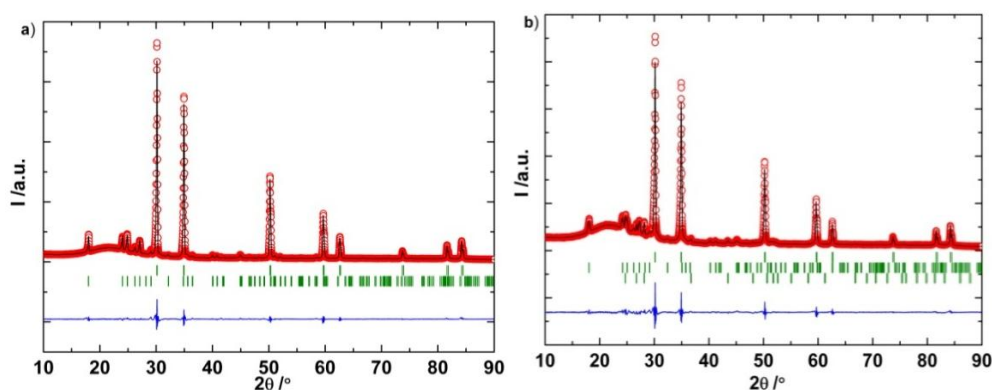
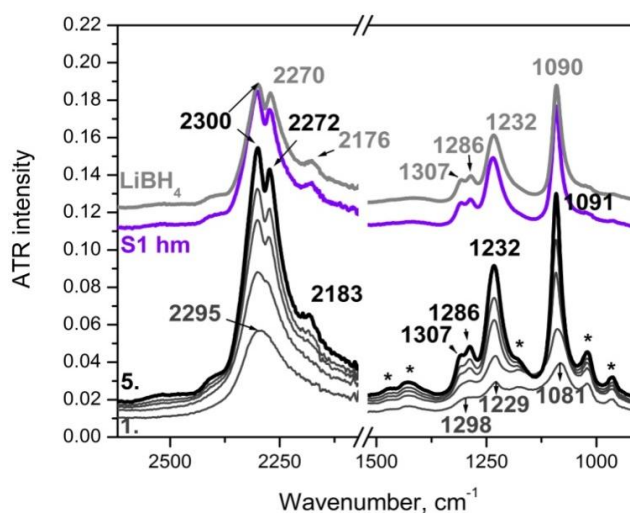


Table 2. Phase composition of the LiBH₄-LiCl hand-milled mixture before and after annealing, as found by Rietveld refinement.

| | Molar fraction, mol% |
|-------------------------------------------------------------------|----------------------|
| LiBH ₄ -LiCl (1:1) S1 hm | |
| LiCl | 44 |
| <i>o</i> -LiBH ₄ | 56 |
| LiBH ₄ -LiCl (1:1) S1 hm, annealed | |
| LiCl | 34 |
| <i>o</i> -Li(BH ₄) _{0.90} Cl _{0.10} | 43 |
| <i>h</i> -Li(BH ₄) _{0.96} Cl _{0.04} | 23 |

The ATR spectrum of the hand-mixed mixture is shown in Figure 6 (violet curve). It is very similar to that of pure LiBH₄ (grey curve). This is in agreement with the presence of pure *o*-LiBH₄ and LiCl in the sample.

Figure 6. Experimental ATR spectra of pure LiBH₄ and LiBH₄-LiCl mixtures, hand-mixed (S1 hm, violet curve) and annealed (S1, black curves 1–5). The spectra 1–5 were obtained at room temperature, within 40 min after annealing and at *ca.* 1 min time step. The curves S1 hm and LiBH₄ are translated vertically for clearness. Peaks marked with * are attributed to impurities.



After annealing, however, the spectrum is strongly modified (Figure 6, black curve 1), but these modifications are not preserved with time. In particular, the spectrum 1 in Figure 6 has one broad peak in the B-H stretching at *ca.* 2400–2100 cm⁻¹, which within a short time (*ca.* 20 min), splits into two (spectra 2–5), narrows, and gains intensity. HBH bending modes in the 1300–1000 cm⁻¹ region are also modified: the peak at 1298 cm⁻¹ splits into two components at 1310–1286 cm⁻¹, and the peaks at 1229 and 1081 cm⁻¹ grow in intensity and shift upwards. The combination modes at 2181 cm⁻¹ and in the 2300–2550 cm⁻¹ regions also gain intensity. These changes in the infrared spectra are similar to those observed [23] in the *in situ* Raman measurements of the LiBH₄ upon heating in the 22–139 °C temperature range, and should be associated with C_{3v} → C_s site symmetry lowering of the BH₄⁻ tetrahedra upon P6₃mc → Pnma phase transformation in LiBH₄. It is important to note that for the *in situ* Raman experiment, the phase transformation was observed during heating and cooling. For this

study, all spectra were obtained at room temperature after the annealing of LiBH_4 with LiCl . This fact evidences the role of Cl in the short-term stabilization of the high temperature hexagonal phase of LiBH_4 . In fact, Arnbjerg *et al.* [12] have demonstrated that the phase transition temperature in LiBH_4 (during cooling) can approach $20\text{ }^\circ\text{C}$, depending on the degree of Cl -substitution. They note that this change in the phase transition temperature indicates a stabilization of the hexagonal phase caused by the incorporation of Cl^- in the LiBH_4 structure.

According to the X-ray diffraction data, which were obtained shortly after the infrared experiment (and therefore better correspond to the curve 5, Figure 6), $o\text{-Li}(\text{BH}_4)_{0.90}\text{Cl}_{0.10}$, phase prevails in this sample, which explains its similarity to the spectrum of pure $o\text{-LiBH}_4$. Note that the computed spectra of $o\text{-LiBH}_4$ and the $o\text{-Li}(\text{BH}_4)_{0.75}\text{Cl}_{0.25}$ are very similar (Figure 4a). Present results are in good agreement with those reported by Arnbjerg *et al.* [12]. In fact, after annealing during cooling, the hexagonal phase found at high temperature is quenched in the mixture. The ortho-to-hexa phase transition is promoted at RT , as evidenced by ATR measurements (Figure 6). During the phase transformation, the Cl^- content in LiBH_4 is strongly reduced and LiCl is formed. The Cl^- content in the orthorhombic phase ($x = 0.10$), observed in PXRD measurements, is in agreement with previous experiments [12], but it turns out higher than that predicted by combined *ab initio* and CALPHAD calculations (Figure 3). As described before, the estimated solubility range is very sensitive to the results of *ab initio* calculation, which would need a more accurate determination of lattice stability in order to fully describe the experimental findings.

3. Calculations

3.1. Ab Initio

Ab initio calculations based on DFT GGA Hamiltonian (PBE) were carried out with the periodic CRYSTAL09 code and localized basis set functions of polarized double- ζ quality. In detail: Li cation was described with a 5–11G(d) basis set ($\alpha_{\text{sp}} = 0.479\text{ bohr}^{-2}$ for the most diffuse shell exponent and $\alpha_{\text{pol}} = 0.600\text{ bohr}^{-2}$ for polarization), while for boron a 6–21G(d) was adopted ($\alpha_{\text{sp}} = 0.124\text{ bohr}^{-2}$ for the most diffuse shell exponent and $\alpha_{\text{pol}} = 0.800\text{ bohr}^{-2}$ for polarization). For hydrogen, a 31G(p) ($\alpha_{\text{sp}} = 0.1613\text{ bohr}^{-2}$ for the most diffuse shell exponent and $\alpha_{\text{pol}} = 1.1\text{ bohr}^{-2}$ for polarization) was considered; for chlorine, a 86–311G basis set was used ($\alpha_{\text{sp}} = 0.125\text{ bohr}^{-2}$ for the most diffuse shell exponent).

Phonons at Γ point in the harmonic approximation were computed to derive the thermodynamic functions by diagonalizing the associated mass-weighted Hessian matrix (for details on the computational procedure see references [31,32]). Grimme's correction to the electronic energy was computed to take dispersion forces into account for all calculations, following the D^* approach described in the literature [33,34]. The enthalpy data were obtained as the electronic energy, including the zero-point energy correction (ZPE), and the thermal factor at the desired temperature.

3.2. CALPHAD

Unary phases (*i.e.*, pure elements) have been described according to the SGTE database [35]. The cubic phase was considered as stoichiometric LiCl , neglecting the possible solubility of LiBH_4 in this

structure. The thermodynamic parameters for this compound ($^{\text{CUBIC}}G(\text{LiCl})$) were taken from the Substance SGTE database [36].

$\text{LiBH}_4\text{-LiCl}$ solid solutions with orthorhombic and hexagonal structures were modeled using two sublattices, the first occupied by Li^+ and the second occupied by Cl^- or by a BH_4^- unit.

As usual, the Gibbs free energy of these solutions can be expressed as [26]:

$$\begin{aligned}\varphi G &= \varphi G^{\text{ref}} - T \cdot S^{\text{id}} + \varphi G^{\text{exc}} \\ \varphi G^{\text{ref}} &= x \cdot \varphi G(\text{LiCl}) + (1-x) \cdot \varphi G(\text{LiBH}_4) \\ S^{\text{id}} &= -R(x \ln(x) + (1-x) \ln(1-x))\end{aligned}$$

where φ represents the phase (orthorhombic or hexagonal), x represents the mole fraction of LiCl , T is the temperature, and G^{ref} , S^{id} , G^{exc} are the reference Gibbs energy, the ideal entropy contribution and the excess contribution to the free energy, respectively.

$^{\text{ORTHO}}G(\text{LiBH}_4)$ was taken from the Substance database. On the basis of *ab initio* calculations, the free energy of orthorhombic LiCl was evaluated as $^{\text{ORTHO}}G(\text{LiCl}) = ^{\text{CUBIC}}G(\text{LiCl}) + A - BT$, where $^{\text{CUBIC}}G(\text{LiCl})$ was taken from the Substance database and $A = 21.8 \text{ kJ mol}^{-1}$ and $B = 7.2 \text{ J K}^{-1} \text{ mol}^{-1}$. As shown in Figure 2, since the *ab initio* calculated enthalpy of mixing is slightly positive and nearly symmetric, the excess Gibbs energy was modeled as a regular solution, giving $^{\text{ORTHO}}G^{\text{exc}} = x(1-x) \cdot \Omega$ with $\Omega = 5.940 \text{ kJ mol}^{-1}$.

Because the thermodynamic function for LiBH_4 reported in the Substance database does not take into account the phase transition [25] from orthorhombic to hexagonal phases occurring at 383 °K , new thermodynamic parameters for the hexagonal LiBH_4 have been evaluated. According to the enthalpy and temperature of transition measured by Price *et al.* [25], the Gibbs free energy of *h*- LiBH_4 has been described as $^{\text{HEX}}G(\text{LiBH}_4) = ^{\text{ORTHO}}G(\text{LiBH}_4) + A - BT$, where $A = 4.4 \text{ kJ mol}^{-1}$ and $B = 11.4 \text{ J K}^{-1} \text{ mol}^{-1}$. Since no experimental data are available for the hexagonal LiCl , $^{\text{HEX}}G(\text{LiCl})$ was evaluated on the basis of *ab initio* calculations as $^{\text{HEX}}G(\text{LiCl}) = ^{\text{CUBIC}}G(\text{LiCl}) + A - BT$, where $A = 15.1 \text{ kJ mol}^{-1}$ and $B = 2.3 \text{ J K}^{-1} \text{ mol}^{-1}$. According to the results of *ab initio* calculations the excess Gibbs energy of the hexagonal solid solution was modeled as a regular solution, giving $^{\text{HEX}}G^{\text{exc}} = x(1-x) \cdot \Omega$ with $\Omega = -4.827 \text{ kJ mol}^{-1}$.

4. Experimental Section

The samples used for the infrared experiments were handled in a nitrogen-filled glove box. As received anhydrous LiCl (Aldrich, purity 98.0%) was additionally dried in a dynamic vacuum at 120 °C and then transferred to the glove box. LiBH_4 (Aldrich, purity 95.0%) was stored in the glove box. The absence of water impurities was controlled by infrared analysis. The sample was thoroughly mixed in the agate mortar in 1:1 molar ratio (this sample is denoted as “S1 hm” in the text). The mixture was then closed in a quartz sample holder and annealed at 250 °C for 24 h in static vacuum. ATR spectra were recorded at room temperature within 40–60 min after annealing (denoted “S1 hm, annealed” in the text).

Infrared spectra were recorded on the single-reflection ALPHA-Platinum ATR (attenuated total reflection) instrument (BRUKER) with diamond crystal accessory. All infrared measurements were held in the glove box, using samples as such, at room temperature. The spectra were obtained in a

4000–400 cm^{-1} range at 2 cm^{-1} resolution. 64 scans were averaged for each spectrum and for the background.

To verify the phase composition of the mixtures after mixing and after annealing, the samples were sealed in 0.5 mm glass capillary and powder X-ray diffraction (PXRD) patterns were obtained in the 10–90° 2θ -region (within 1 h after treatment). PXRD patterns were collected with a X'Pert PRO MPD diffractometer (PANalytical), with a Cu K_α wavelength. Patterns were collected in Debye-Scherrer geometry at room temperature, placing the capillary with the sample on the rotating goniometer. PXRD data were analyzed by Rietveld refinement using FullProf Suite [37]. The background was described by linear interpolation between selected points, while Gauss profile functions were used to fit the diffraction peaks. In the refinements, scale factors, unit cell parameters, profile parameters (U , V , W), the overall temperature factor and the background were refined.

5. Conclusions

Dissolution of LiCl in the hexagonal and orthorhombic LiBH_4 were studied with *ab initio* calculations, thermodynamic modeling and infrared spectroscopy. According to our calculations, the enthalpy of mixing for the hexagonal phase is slightly negative, while that of the orthorhombic phase is positive. Overall, the thermodynamic effect of Cl substitution into the LiBH_4 is negligible. Although computed infrared spectra do not give the possibility of punctual comparison and assignment of $\text{LiBH}_4\text{-Cl}$ solid solution modes, they clearly show that Cl does not affect the positions of BH_4^- fundamentals strongly. A minor effect is therefore expected for the stability of LiBH_4 if the correlation between these properties is believed to exist. To our knowledge, this is the first infrared study of the phase transition from *h*- to *o*- LiBH_4 . The phase transition is observed at room temperature, due to the fact that the presence of Cl either decreases phase transition temperature or slows down phase transition kinetics. Infrared spectra of the solid solution, obtained at ambient temperature shortly after annealing, have a profile characteristic for the high temperature hexagonal phase of LiBH_4 , where BH_4^- anions possess higher site symmetry. These spectra are also remarkably similar to those of $\text{LiBH}_4\text{-LiBr}$ and $\text{LiBH}_4\text{-LiI}$ solid solutions, where halides dissolve at high temperature in the hexagonal phase of LiBH_4 and preserve this structure for a long time (months) at ambient temperature.

Acknowledgments

The authors thank Giuseppe Spoto (University of Turin) for useful discussion and critical reading of the manuscript. European Commission (contract NMP-2008-261/FLYHY, grant Agreement number 226943) financial support is highly appreciated.

References

1. Yin, L.; Wang, P.; Fang, Z.; Huiming, C. Thermodynamically tuning LiBH_4 by fluorine anion doping for hydrogen storage: A density functional study. *Chem. Phys. Lett.* **2008**, *450*, 318–321.
2. Corno, M.; Pinatel, E.; Ugliengo, P.; Baricco, M. A computational study on the effect of fluorine substitution in LiBH_4 . *J. Alloys Compd.* **2011**, *509S*, S679–S683.

3. Brinks, H.W.; Fossdal, A.; Hauback, B.C. Adjustment of the stability of complex hydrides by anion substitution. *J. Phys. Chem. C* **2008**, *112*, 5658–5661.
4. Au, M.; Spencer, W.; Jurgensen, A.; Zeigler, C. Hydrogen storage properties of modified lithium borohydrides. *J. Alloys Compd.* **2008**, *462*, 303–309.
5. Zhang, B.J.; Liu, B.H. Hydrogen desorption from LiBH₄ destabilized by chlorides of transition metal Fe, Co, and Ni. *Int. J. Hydrogen Energy* **2010**, *35*, 7288–7294.
6. Lee, J.Y.; Lee, Y.-S.; Suh, J.Y.; Shim, J.H.; Cho, Y.W. Metal halide doped metal borohydrides for hydrogen storage: The case of Ca(BH₄)₂–CaX₂ (X = F, Cl) mixture. *J. Alloys Compd.* **2010**, *506*, 721–727.
7. Rude, L.H.; Nielsen, T.K.; Ravnsbaek, D.B.; Boesenberg, U.; Ley, M.B.; Richter, B.; Arnbjerg, L.M.; Dornheim, M.; Filinchuk, Y.; Besenbacher, F.; *et al.* Tailoring properties of borohydrides for hydrogen storage: A review. *Phys. Status Solidi (a)* **2011**, *208*, 1754–1773.
8. Matsuo, M.; Remhof, A.; Martelli, P.; Caputo, R.; Ernst, M.; Miura, Y.; Sato, T.; Oguchi, H.; Maekawa, H.; Takamura, H.; *et al.* Complex hydrides with (BH₄)⁽⁻⁾ and (NH₂)⁽⁻⁾ anions as new lithium fast-ion conductors. *J. Am. Chem. Soc.* **2009**, *131*, 16389–16391.
9. Matsuo, M.; Nakamori, Y.; Orimo, S.; Maekawa, H.; Takamura, H. Lithium superionic conduction in lithium borohydride accompanied by structural transition. *Appl. Phys. Lett.* **2007**, *91*, 224103–224105.
10. Maekawa, H.; Matsuo, M.; Takamura, H.; Ando, M.; Noda, Y.; Karahashi, T.; Orimo, S.I. Halide-stabilized LiBH₄, a room-temperature lithium fast-ion conductor. *J. Am. Chem. Soc.* **2009**, *131*, 894–895.
11. Matsuo, M.; Takamura, H.; Maekawa, H.; Li, H.W.; Orimo, S. Stabilization of lithium superionic conduction phase and enhancement of conductivity of LiBH₄ by LiCl addition. *Appl. Phys. Lett.* **2009**, *94*, 084103–084105.
12. Arnbjerg, L.M.; Ravnsbaek, D.B.; Filinchuk, Y.; Vang, R.T.; Cerenius, Y.; Besenbacher, F.; Jorgensen, J.E.; Jakobsen, H.J.; Jensen, T.R. Structure and dynamics for LiBH₄-LiCl solid solutions. *Chem. Mater.* **2009**, *21*, 5772–5782.
13. Oguchi, H.; Matsuo, M.; Hummelshoj, J.S.; Vegge, T.; Norskov, J.K.; Sato, T.; Miura, Y.; Takamura, H.; Maekawa, H.; Orimo, S. Experimental and computational studies on structural transitions in the LiBH₄-LiI pseudobinary system. *Appl. Phys. Lett.* **2009**, *94*, 141912/1–141912/3.
14. Rude, L.H.; Groppo, E.; Arnbjerg, L.M.; Ravnsbaek, D.B.; Malmkjaer, R.A.; Filinchuk, Y.; Baricco, M.; Besenbacher, F.; Jensen, T.R. Iodide substitution in lithium borohydride, LiBH(4)-LiI. *J. Alloys Compd.* **2011**, *509*, 8299–8305.
15. Rude, L.H.; Zavorotynska, O.; Arnbjerg, L.M.; Ravnsbaek, D.B.; Malmkjaer, R.A.; Grove, H.; Hauback, B.C.; Baricco, M.; Filinchuk, Y.; Besenbacher, F.; *et al.* Bromide substitution in lithium borohydride, LiBH(4)-LiBr. *Int. J. Hydrogen Energy* **2011**, *36*, 15664–15672.
16. Dovesi, R.; Saunders, V.R.; Roetti, C.; Zicovich-Wilson, C.M.; Pascale, F.; Civalleri, B.; Doll, K.; Harrison, N.M.; Bush, I.J.; D'Arco, P.; *et al.* *CRYSTAL2009 User's Manual*; University of Torino: Torino, Italy, 2009.
17. Fonnelløp, J.E.; Corno, M.; Grove, H.; Pinatel, E.; Sorby, M.H.; Ugliengo, P.; Baricco, M.; Hauback, B.C. Experimental and computational investigations on the AlH(3)/AlF(3) system. *J. Alloys Compd.* **2011**, *509*, 10–14.

18. Bergerhoff, G.; Brown, I.D. *Crystallographic Databases*; Allen, F.H., Bergerhoff G., Sievers, R., Eds.; International Union of Crystallography: Chester, UK, 1987.
19. Zavorotynska, O.; Corno, M.; Damin, A.; Spoto, G.; Ugliengo, P.; Baricco, M. Vibrational properties of MBH(4) and MBF(4) crystals (M = Li, Na, K): A combined DFT, infrared, and raman study. *J. Phys. Chem. C* **2011**, *115*, 18890–18900.
20. Lide, D.R. *CRC Handbook of Chemistry and Physics*, 88th ed.; CRC: Boca Raton, FL, USA, 2007.
21. Hartman, M.R.; Rush, J.J.; Udovic, T.J.; Bowman, R.C.; Hwang, S.J. Structure and vibrational dynamics of isotopically labeled lithium borohydride using neutron diffraction and spectroscopy. *J. Solid State Chem.* **2007**, *180*, 1298–1305.
22. Miwa, K.; Ohba, N.; Towata, S.; Nakamori, Y.; Orimo, S. First-principles study on lithium borohydride LiBH₄. *Phys. Rev. B* **2004**, *69*, 245120/1–245120/8.
23. Gomes, S.; Hagemann, H.; Yvon, K. Lithium boro-hydride LiBH₄ II. Raman spectroscopy. *J. Alloys Compd.* **2002**, *346*, 206–210.
24. El Kharbachi, A.; Nuta, I.; Hodaj, F.; Baricco, M. Above room temperature heat capacity and phase transition of lithium tetrahydroborate. *Thermochim. Acta* **2011**, *520*, 75–79.
25. Price, T.E.C.; Grant, D.M.; Telepeni, I.; Yu, X.B.; Walker, G.S. The decomposition pathways for LiBD₄-MgD₂ multicomponent systems investigated by in situ neutron diffraction. *J. Alloys Compd.* **2009**, *472*, 559–564.
26. Lukas, H.L.; Fries, S.G.; Sundman, B. *Computational Thermodynamics*; Cambridge University Press: Cambridge, UK, 2007.
27. Andresen, E.R.; Gremaud, R.; Borgschulte, A.; Ramirez-Cuesta, A.J.; Zuttel, A.; Hamm, P. Vibrational Dynamics of LiBH₄ by Infrared Pump-Probe and 2D Spectroscopy. *J. Phys. Chem. A* **2009**, *113*, 12838–12846.
28. Harvey, K.B.; McQuaker, N.R. Low temperature infrared and raman spectra of lithium borohydride. *Can. J. Chem.* **1971**, *49*, 3282–3286.
29. Orimo, S.; Nakamori, Y.; Zuttel, A. Material properties of MBH₄ (M=Li, Na, and K). *Mater. Sci. Eng. B* **2004**, *108*, 51–53.
30. Hagemann, H.; Filinchuk, Y.; Chernyshov, D.; van Beek, W. Lattice anharmonicity and structural evolution of LiBH₄: an insight from Raman and X-ray diffraction experiments. *Phase Transit.* **2009**, *82*, 344–355.
31. Pascale, F.; Zicovich-Wilson, C.M.; Gejo, F.L.; Civalleri, B.; Orlando, R.; Dovesi, R. The calculation of the vibrational frequencies of crystalline compounds and its implementation in the CRYSTAL code. *J. Comput. Chem.* **2004**, *25*, 888–897.
32. Zicovich-Wilson, C.M.; Torres, M.R.; Pascale, F.; Valenzano, L.; Orlando, R.; Dovesi, R. *Ab initio* simulation of the IR spectra of pyrope, grossular, and andradite. *J. Comput. Chem.* **2008**, *29*, 2268–2278.
33. Civalleri, B.; Zicovich-Wilson, C.M.; Valenzano, L.; Ugliengo, P. B3LYP augmented with an empirical dispersion term (B3LYP-D*) as applied to molecular crystals. *CrystEngComm* **2008**, *10*, 405–410.
34. Grimme, S. Semiempirical GGA-type density functional constructed with a long-range dispersion correction. *J. Comput. Chem.* **2006**, *27*, 1787–1799.

35. Dinsdale, A. SGTE data for pure elements. *Calphad* **1991**, *15*, 317–425.
36. SGTE substance database V 4.1. Available online: http://www.crct.polymtl.ca/fact/documentation/sgps_list.htm (accessed on 2 February 2012).
37. Rodriguez-Carvajal, J. *FULLPROF SUITE: LLB*; Sacley & LCSIM: Rennes, France, 2003.

© 2012 by the authors; licensee MDPI, Basel, Switzerland. This article is an open access article distributed under the terms and conditions of the Creative Commons Attribution license (<http://creativecommons.org/licenses/by/3.0/>).